Article:
Settle, A., Mishra, R., Shanmugam, R.-K. et al. (2026) Co-solute effects reveal the nature of weak forces governing GLP-1 oligomers stability. Journal of Biological Chemistry. 111223. ISSN: 0021-9258

https://doi.org/10.1016/j.jbc.2026.111223

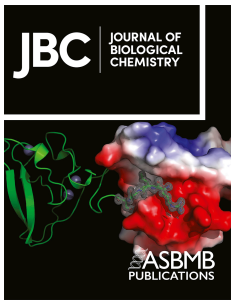

Co-solute Effects Reveal the Nature of Weak Forces Governing GLP-1 Oligomers Stability

Anyah Settle, Rahul Mishra, Ramesh-Kumar Shanmugam, Viv Lindo, Nathan B.P. Adams, Thomas A. Jowitt, Tuck Seng Wong, Barbara Ciani

PII: S0021-9258(26)00093-1

DOI: https://doi.org/10.1016/j.jbc.2026.111223

Reference: JBC 111223

To appear in: *Journal of Biological Chemistry*

Received Date: 16 May 2025

Revised Date: 26 November 2025

Accepted Date: 14 January 2026

Please cite this article as: Settle A, Mishra R, Shanmugam RK, Lindo V, Adams NBP, Jowitt TA, Wong TS, Ciani B, Co-solute Effects Reveal the Nature of Weak Forces Governing GLP-1 Oligomers Stability, *Journal of Biological Chemistry* (2026), doi: https://doi.org/10.1016/j.jbc.2026.111223.

Title

Co-solute Effects Reveal the Nature of Weak Forces Governing GLP-1 Oligomers Stability

Anyah Settle[1], Rahul Mishra[2], Ramesh-Kumar Shanmugam[3], Viv Lindo[2], Nathan B P Adams[4], Thomas A Jowitt[5], Tuck Seng Wong[6*] and Barbara Ciani[1*].

1 Centre for Chemical Biology, School of Mathematical and Physical Science, University of Sheffield, Sheffield S3 7HF, UK

2. BioPharmaceuticals Development, Analytical Sciences, AstraZeneca, Cambridge CB2 0AA, United Kingdom, UK

3. Biopharmaceutical Development, Dosage Form Design and Development, AstraZeneca, Cambridge CB2 0AA, UK

4. NanoTemper Technologies GmbH, Tölzer Str 1, 81379, Munich, Germany

5. Wellcome Centre for Cell-Matrix Research, Faculty of Biology, Medicine and Health, Manchester Academic Health Science Centre, University of Manchester, Manchester M13 9PT, UK

6. School of Chemical, Materials and Biological Engineering, University of Sheffield, Sir Robert Hadfield Building, Mappin Street, Sheffield, S1 3JD, UK

Keywords

GLP-1, protein aggregation, colloidal stability, physical stability, amyloid, self-assembly

*Correspondence to: b.ciani@sheffield.ac.uk, t.wong@sheffield.ac.uk

List of Abbreviations

GLP-1 (Glucagon-like peptide-1), DPP-IV (Dipeptidyl peptidase IV), GLP-1RAs (GLP-1 Receptor Agonists), DLS (Dynamic light scattering), DSF (Differential scanning fluorimetry), SV-AUC (sedimentation velocity analytical ultracentrifugation, TFA (Trifluoroacetic acid), CD (Circular dichroism), AF4 (Asymmetric flow field flow fractionation), SEC (Size exclusion chromatography), NaCl (sodium chloride).

Abstract

Glucagon-like peptide-1 (GLP-1) is an incretin hormone widely used to manage diabetes and obesity, through its ability to regulate glucose homeostasis. Clinically relevant GLP-1 sequences form oligomeric states. Uncontrolled oligomer formation can drive fibril formation, posing challenges such as difficulty in controlling drug dosage, loss of activity, or toxicity, as the aggregates can be immunogenic and/or can form amyloids. Here, we used combined measurements of colloidal and conformational stability to characterise the intermolecular interactions underpinning the physical status of the GLP-1 7-37 amide (GLP-1am), at pharmaceutically relevant high concentrations. We focus on less explored conditions, around pH 5, mimicking the environment within native cellular secretory granules, where the hormone is also densely packed. Co-solutes allowed us to interfere with weak interactions affecting peptide self-association into soluble oligomers, and the conversion into aggregates and fibrils. We show that GLP-1am exists as soluble oligomers that assemble into nanosheets over the timescale of hours, in quiescent conditions. Aggregation proceeded via a nucleation-dependent mechanism, with its rate correlating to the magnitude of attractive intermolecular interactions. It was accelerated by ionic co-solutes, indicating a key role for screening of electrostatic interactions in modulating peptide–peptide attraction and assembly. The rate of aggregation was also pH-dependent, with rates being slower at pH 5 than pH 8. Notably, the addition of proline, as a co-solute, delayed the onset of GLP-1am aggregation in a pH-dependent manner. Thus, in quiescent conditions, GLP-1am forms discrete soluble oligomers capable of organising into ordered nanostructures rather than amyloid fibrils.

Introduction

Glucagon-like peptide-1 (GLP-1) is an incretin hormone that plays a crucial role in regulating glucose homeostasis. The GLP-1 peptide binds to the glucagon receptor, a member of the B family of seven transmembrane G-protein-coupled receptors (GPCR) (1). This receptor is an effective target for lowering elevated blood glucose levels associated with type 2 diabetes (2). GLP-1 receptor agonists (GLP-1RAs) stimulate insulin secretion, suppress glucagon release, and delay gastric emptying in a glucose-dependent manner (3). However, the native peptide sequences have a short circulating lifetime ($t_{1/2}$ ~ 2 minutes after intravenous administration) due to cleavage of the peptide's N-terminus by dipeptidyl peptidase IV (DPP-IV), resulting in deactivation (2). Strategies for improving the half-life and uptake of GLP-1RAs include the addition of lipids and sequence modifications, such as substitution with non-canonical amino acids at protease cleavage sites. In the case of liraglutide, a common GLP-1 RA antidiabetic and obesity medication, adding a lipid tail increases the half-life to 9-13 hours (4).

GLP-1RAs have demonstrated broader benefits, such as significantly reducing the risk of heart failure, atherosclerosis, and hypertension (5). Consequently, there is a broad interest in providing agonists, which are more stable and effective under physiological conditions both prior to and following administration.

GLP-1 peptides have a tendency to self-associate into reversible oligomers leading to delayed absorption into systemic circulation, where monomers bind to albumin (6, 7). Oligomerisation improves stability and activity (8, 9) when maintained in circulation. Similarly, GLP-1's biological activity is regulated by the slow release of monomers from hormone fibrils stored in the secretory granules (10). Due to the propensity for self-association, GLP-1RAs are challenging to formulate in conditions that retain physical stability during storage (11) and avoid aggregated states that could compromise therapeutic efficacy (12).

Since the discovery of GLP-1's therapeutic potential, the mechanisms of aggregation (13–16) have been explored (11, 14). However, a gap in understanding remains regarding which intermolecular interactions underpin GLP-1 oligomerisation and how co-solutes can influence its aggregation propensity. This knowledge is crucial for designing strategies to either develop next-generation GLP-1RAs and/or select solution conditions that control oligomeric species and inhibit aggregation, thus preventing the formation of immunogenic species.

The initial step in the kinetics of protein self-association leading to either amorphous aggregation or organised fibril formation involves the formation of soluble oligomers. The pathway taken depends on the solution conditions experienced by the polypeptide chain, which can favour β amyloid structures (17, 18).

GLP-1 7-37, 7-36 amide and 7-37 amide show similar receptor affinity and activation but slightly different pathways to amyloid fibrillation (19, 20), which have been studied around physiological pH and at low peptide concentrations (21, 22). GLP-1 7-37 amide (GLP-1am)

self-associates at low concentrations (0.3 mg mL^{-1}) upon mechanical agitation, forming distinct oligomers containing 3-4 peptide subunits (22). These oligomers appear thermally stable and are not impacted by sonication but denature in the presence of anionic surfactants, whilst non-ionic surfactants drive oligomerisation further. However, most commercial human GLP-1RA formulations consist of highly concentrated solutions (4) (1.3 to 6 mg mL^{-1}) at mildly alkaline pH, while native GLP-1 is stored in the crowded environment of cellular secretory granules at mildly acidic pH. This ensures both slow release and controlled activity. Importantly, physical stability studies of GLP-1 in formulation-relevant and natural storage conditions are lacking, and this knowledge could provide the basis for precise control of GLP-1 self-association and monomer release from its assembled state.

The physical behaviour of a protein in solution is determined by its colloidal and conformational stabilities, both of which are regulated by inter and intramolecular non-covalent interactions (17). Dynamic light scattering (DLS) and determination of the diffusion interaction parameter (k_D) (23) are methods of choice to quantify colloidal stability. The k_D directly correlates with protein diffusivity in solution, which in turn, depends on the magnitude of protein-protein interactions (24). Nano differential scanning fluorimetry (nanoDSF) allows the measurement of conformational stability by following protein unfolding induced by temperature via intrinsic fluorescence.

Herein, we report the use of high-throughput combined light scattering (DLS and turbidity), and nanoDSF measurements to characterise the physical stability of GLP-1am at concentrations relevant to therapeutic formulations, at secretory granule-relevant pH (pH 5.5-6), under quiescent conditions (25).

We unravel the intermolecular interactions driving peptide oligomerisation using selected, pharmaceutically relevant co-solutes, and characterise how biologically-relevant storage conditions control the morphology and the kinetics of monomer self-assembly to form GLP-1am fibrils.

We show that in the absence of mechanical stress, GLP-1am forms large nano structures as opposed to fibrils. Sodium chloride (NaCl) drives steady aggregation of GLP-1am, whilst the salt form of arginine (arginine.HCl) drive self-association at high co-solute concentrations. Significantly, proline appears to slow down the growth of aggregates by stabilising early oligomeric species. Thus, we present how the impact of co-solutes on GLP-1am self-assembly gives indications on the nature of the intermolecular interactions responsible for the early stages of self-association.

Results

Attractive interactions govern GLP-1am oligomer growth, in a pH-dependent manner.

We employed simultaneous measurements of size distribution, thermal unfolding, fluorescence, scattering and turbidity to quantify the colloidal and conformational stability of GLP-1am in acetate buffer at pH 5, at concentrations from 1 to 8 mg mL^{-1}. The size distribution profile of GLP-1am dilutions from a high concentration stock showed the presence of several oligomeric species (SF1), some persistent, and some present only at the highest concentration (100 nm > R_h < 1000 nm; SF1E). The hydrodynamic radius (R_h) of the main GLP-1am species (SF1, peak 1) increased with increasing peptide concentration, from 2.8 to 3.8 nm between 1 to 8 mg mL^{-1} (Figure 1A). The estimated R_h of GLP-1am (~2.15 nm), calculated from its hydrodynamic volume using the convex method (26) (PDB 3IOL) suggested that the main species (peak 1) likely represents a combination of monomer and oligomers with sizes too similar to be resolved by DLS. Although high-throughput measurements indicated that the main population (peak 1) of GLP-1am is monodisperse (Figure 1B), detection at a different scattering angle (SF2A, B) confirmed GLP-1am was polydisperse (Table S1). The concentration-dependent data allowed us to calculate the diffusion interaction parameter (k_D) to quantify the interactions between GLP-1am molecules in the population with R_h in the range of 2.8 – 3.8 nm (Figure 1C; k_D value around $–29 \pm 4$ mL g^{-1}). The sign and magnitude of the k_D value determine the intermolecular interactions: negative values indicate attraction, while positive values indicate repulsion (27, 28). For GLP-1am in acetate buffer at pH 5 the k_D was negative, a finding consistent across high and low-throughput measurements (SF2C, k_D value around $–32 \pm 9$ mL g^{-1}). This confirmed the presence of attractive interactions at pH 5, albeit weaker than those observed at pH 8 (SF2D-F; $k_D = –42 \pm 8$ mL g^{-1}).

To quantify the thermal stability of oligomeric species, we measured the change of intrinsic fluorescence of aromatic residues with thermal stress. From 20 to ~60 °C, GLP-1am showed a linear increase in the ratio of fluorescence intensity at 350 nm to 330 nm (F_{350}/F_{330}), indicating unfolding of weakly associated peptide oligomers (SF3A). At peptide concentrations of 4 mg mL^{-1} and above, we observed a sharp decrease in the F_{350}/F_{330} with a simultaneous increase in scattering intensity (SF3B) and of turbidity (SF3C) from ~55 °C (SF3A, D). These events suggested a burying of the aromatic residues due to the formation of large species, which occurred at increasingly lower temperatures with increasing peptide concentration (Figure 1D-E). The temperature marking this assembly event ($IP_{F_{agg}}$), coincided with the first appearance of turbidity (Figure 1F; SF3D) a result of the formation of particles > 12.5 nm. The turbidity signal showed two distinct transitions (T_{agg1} and T_{agg2}), indicating the growth of oligomers, with larger species being more thermally stable at higher concentrations (T_{agg1}, Figure 1E-F and SF3C). This event coincided with the appearance of a second species in the size distribution during the thermal ramp, just as the smaller species disappeared around ~57°C. This new species, around 100 nm R_h, became more populated until it also disappeared at ~ 76 °C (SF3E) at which point the intensity of scattered light became too great to measure using DLS.

We utilised low-throughput fluorescence measurements to further probe the environments of the aromatic residues in GLP-1am. The emission of the freshly dissolved GLP-1am at 340 nm (SF3F) suggested that the aromatic residues were partially buried in a hydrophobic environment. confirming the presence of oligomers (29). After days of incubation without agitation, at 25 °C, GLP-1am aromatic residues displayed a decrease in emission intensity at both pH 5 and pH 8 (SF3F, G) with a small blue shift of 2 nm in emission, highlighting further changes to GLP-1am oligomers conformation.

Lastly, we sought to define how solution conditions impact the self-association behaviour of GLP-1am by exploiting electrophoretic, spectroscopic, and chromatographic methods across a range of pH conditions. The ζ-potential, which describes the surface charge, was near zero for GLP-1am at approximately pH 6.2 (SF4A), close to the previously measured isoelectric point of 6.8 (22). The surface charge followed the curve of the net charge between pH 3.7 and 6, but then declined rapidly between 6 and 8. Overall, the of ζ-potential values for GLP-1am fell within the ±30 mV range, indicating poor colloidal stability, and a general tendency to self-association between pH 3 and 8. This was consistent GLP-1am being larger than expected for a monomer at any pH (SF4B), with the smallest R_h measured at pH 4 and the largest at pH 7. The polydispersity was invariant with respect to pH, except at pH 8 when it decreased below 16% (SF4C), but with large variation in hydrodynamic size. AF4-MALS reported GLP-1am as a large oligomer between 1 and 4 mg mL^{-1} (Table S2). Consistent with the hydrodynamic measurements, far-UV circular dichroism (CD) showed that GLP-1am helical content at pH 4 is lower than that at pH 5 and 8 (SF4D). SEC was used to estimate GLP-1am existed as a dimer at pH 8 at 0.3 mg mL^{-1} (SF4E, Table S4).

Thus, GLP-1am shows poor colloidal stability across a wide pH range providing a driving force for self-association. This assembly process is concentration-dependent, resulting in differential thermal stabilities where small oligomers become less stable with concentration, while larger aggregates become more stable. GLP-1am oligomer size and conformation are also pH-dependent, with attractive interactions driving self-association being weaker at pH 5 than pH 8.

The impact of salt and osmolytes on the physical stability of GLP-1am

To probe the nature of the intermolecular interactions that drive GLP-1am self-association, we examined the effect of co-solutes on the physical stability of GLP-1am at pH 5. NaCl was chosen to disrupt electrostatic interactions, whilst arginine.HCl and proline were employed to interfere with the formation of oligomers driven by a combination of electrostatics, cation−π and hydrophobic interactions (30).

Characterisation of the colloidal status of GLP-1am by DLS showed a varying effect on its hydrodynamic size depending on the co-solute. Increasing the NaCl concentration led to a large increase in the R_h of GLP-1am. The effect of NaCl was also greater at higher concentrations of GLP-1am, whose size increased almost linearly with salt concentration (Figure 2A). In contrast, the impact of arginine.HCl was highly dependent on peptide and co-solute concentration (Figure 2B). The R_h of GLP-1am decreased up to 50 mM arginine.HCl and GLP-1am concentrations lower than 4 mg mL^{-1}. Conversely, the R_h increased slightly up to 100 mM co-solute above 4 mg mL^{-1} GLP-1am but remained smaller

than that for acetate alone. The similarity between the impact of NaCl and arginine.HCl on GLP-1am size is likely due to their similar charge screening ability when they are at sufficiently high concentrations. In contrast, at low concentrations, only arginine.HCl can provide some colloidal stabilisation, possibly by preferentially interacting with aromatic sidechains, a similar mechanism observed in larger proteins (31).

Proline cannot interfere with ionic interactions; thus, we hypothesised proline would only have an impact if hydrophobic interactions play a role in GLP-1am self-association. The effect of proline on GLP-1am size appeared negligible in comparison to the effect of ionic co-solutes (Figure 2C). However, we observed a pooled effect of proline that led to a modest but statistically significant reduction in R_h, across most GLP-1am concentrations (mean R_h 3.22 nm vs mean R_h 3.43 nm for GLP-1am in proline and acetate, respectively; standard errors 0.03 nm and 0.07 nm for measured R_h in proline and acetate, respectively). At peptide concentrations of 2 mg mL^{-1} and above, there was a consistent decrease in GLP-1am hydrodynamic radius in the presence of proline in comparison to that in acetate buffer alone. This effect, though small in magnitude, was consistent across conditions; thus, proline seems to favour assemblies with a smaller average size between 2 and 8 mg mL^{-1} GLP-1am.

Characterisation of the thermal stability of GLP-1am with nanoDSF did not show any significant effect by the co-solutes on peptide unfolding profiles (SF5). However, the effect of co-solutes on the mid-point temperature of aggregation, IP_{Fagg} was clear. The decline in IP_{Fagg} , accompanied by the simultaneous increase in turbidity, and peptide size increased with increasing NaCl concentration (Figure 2D, SF5A-E). Thus, NaCl promoted the formation of large aggregated species at lower temperatures than in buffer alone. In the presence of arginine.HCl, the GLP-1am IP_{Fagg} showed a small increase at 12.5 mM, followed by a subsequent decrease that plateaued at 50 mM (Figure 2E, SF5F-L). In comparison to NaCl, arginine.HCl displayed a shallower decrease of the IP_{Fagg} (1°C for arginine.HCl vs 2 °C for NaCl, compare Figure 2D with 2E). Similarly to arginine.HCl, IP_{Fagg} increased up to 100 mM proline concentration, suggesting that proline reduces the tendency of GLP-1am to self-associate with temperature. This effect was less obvious at 8 mg mL^{-1} GLP-1am, where, perhaps, interactions between GLP-1am molecules were predominant (Figure 2F, SF5J-O). It was also apparent that the higher the peptide concentration, the lower the turbidity onset temperature, which is typical of nucleation-dependent mechanisms (Figure 2G-I, Figure 5G).

Subsequently, we sought to understand how co-solutes corresponded to the peptide's propensity to form high-molecular weight species. AF4-MALS and SEC indicated that GLP-1am at pH 5 contained dimeric and trimeric species, up to 2 mg mL^{-1}, alongside aggregates that could not be recovered (Figure 3A, Table S2, S4). Sedimentation velocity analytical ultracentrifugation (SV-AUC) was used to characterise the effect of proline on the formation of large GLP-1am species. SV-AUC showed that whilst proline had a small effect on GLP-1am oligomer formation at 2 mg mL^{-1} peptide (Figure 3B, Table S3), it could prevent the formation of the largest aggregates at a higher peptide concentration. When proline was added to 4 mg mL^{-1} GLP-1am, the number of oligomeric species reduced from three (4, 9 and 14-mers) to two, with the loss of the 14-mer population (Figure 3C; Table S3). To enable direct comparison and to observe the true effect of proline, each 4 mg mL^{-1} GLP-1am sample was prepared from the same stock solution with and without proline. Thus, the loss of the

14-mer demonstrates unequivocally that the reduction reflects a true effect, suggesting that proline likely slowed down the self-association of GLP-1am.

Oligomer growth kinetics, monitored by apparent absorbance at 350 nm, at 25 °C, showed the size of GLP-1am increased faster when arginine.HCl and NaCl were included in the buffer (Figure 3D, E). In contrast to ionic co-solutes, GLP-1am had a slightly delayed onset of turbidity in the presence of proline, which plateaued at lower absorbances (Figure 3D, E). Kinetic measurements were performed using batches purchased from GL Biochem (batch 1) and GenScript (batch 2). The effects of co-solutes on the rate of peptide aggregation were reproducible across peptide preparations (compare with Figure 3D, E with SF7A-C), even though absolute rates were batch-dependent. Adding small amounts of seeds (SF7B, C) or increasing peptide concentration (SF7D and compare SF7A with E) accelerated the aggregation of GLP-1am in both batches, consistent with a nucleation-dependent self-assembly pathway. Albeit to a lesser extent than its salt form, zwitterionic arginine also accelerated GLP-1am aggregation (SF7E). The kinetics were found to be faster at pH 8 than at pH 5, reflecting the greater magnitude of the previously discussed k_D value and, thus, stronger attractive interactions. Oligomer growth was also faster at pH 8 in comparison to pH 5, reflecting the stronger attractive interactions as quantified by the k_D. Notably, the effect of proline was pH-dependent since the addition of proline to GLP-1am at pH 8 had no impact on the aggregation rate (SF7F). Overall, the growth kinetics were repeatable over different days within the same batch (SF7G). Oligomer growth kinetics were supported by SV-AUC of 4 mg mL^{-1} GLP-1am assembled over 18 hours, at 25 ºC, which showed the higher molecular weight species were slightly smaller when proline was present (SF7H and Table S3). Importantly, GLP-1am formed amyloid-like fibrils only when incubated for days with agitation (SF7I).

The T_{agg1} trends measured upon changing temperature, with co-solutes, recapitulated the general propensity of GLP-1am to oligomerise at constant temperature. Whilst arginine.HCl generally decreased T_{agg1}, proline raised this value across concentrations (Figure 4A, B). Ultimately, none of the co-solutes raised the T_{agg1} for the highest GLP-1am concentration (Figure 4C). Interestingly, ionic co-solutes displayed only one turbidity transition upon changing temperature, rather than the two observed with proline or buffer alone (SF6). The T_{agg1} trends also reflected the ability of each co-solute to decrease or increase the k_D for GLP-1am, with proline being the most effective in reducing attractive interactions (Figure 4D). To rationalise the effect of proline on GLP-1am oligomer growth into aggregates, we looked at oligomer size and conformation, in the presence and absence of proline. At low peptide concentration, SEC identified the dimer/trimer tipping point around 2 mg mL^{-1} peptide (Table S4). Proline appeared to favour GLP-1am dimers, compared to the trimers observed in buffer alone (Figure 4E, Table S4). We then used CD to quantify the conformation of GLP-1am oligomers with and without proline. Near-UV CD absorption revealed that fresh GLP-1am adopts a distinct tertiary structure that constrains aromatic residues (Figure 4F). The near UV CD signal at 290 nm was reduced in the presence of proline, suggesting this co-solute promotes a change of environment for aromatic sidechains. Taken together, the SEC and CD data suggest that proline favours smaller GLP-1am sizes at pH 5.

Lastly, we examined the morphology of the GLP-1am aggregates formed after overnight incubation at 25 °C, under quiescent conditions. In contrast to the amyloid fibrils formed by GLP-1am at low concentration over days, with agitation (Figure 3F and (22)), GLP-1am formed straight and flat nanosheets (Figure 5A). These nanosheets appeared shorter and more geometrically defined when arginine.HCl (Figure 5B) and proline were included in the buffer (Figure 5C). At pH 8, the nanosheets spanned a broader distribution, exhibiting two populations with distinct widths (SF8A, B). The morphology of the mature nanosheets was identical across peptide batches and pH conditions (SF8C,D), suggesting that these structures are favoured by either higher peptide concentration, or the lack of mechanical stress during assembly . Analysis of the width distribution revealed that nanostructures structures formed at pH 5 (Figure 5D) have a narrower distribution than those formed in arginine.HCl (Figure 5E), whereas proline generated nanosheets more homogeneous in width (Figure 5F). Interestingly, 200 mM proline promoted populations with two distinct width distributions: one with narrower nanosheets than those observed at 100 mM proline, and one distribution with widths similar to those promoted by arginine.HCl.
In summary, these results show that proline modulates the balance between oligomer formation and growth. GLP-1am oligomers formed in the presence of proline likely adopt a conformation less capable of growing into larger structures over time, and form more homogeneous nanostructures than in buffer alone.

Discussion

GLP-1am self-assembles into organised nanosheets in quiescent conditions, with pH-dependent kinetics.

We showed that GLP-1am self-associates into soluble oligomers at pH 5, with the oligomer size increasing with increasing peptide concentration. The kinetics of aggregation at 25°C are concentration-dependent, which is consistent with a nucleation-dependent mechanism, as reported previously (31). GLP-1am aggregation is accelerated at pH 8, with 8 mg mL^{-1} of GLP-1am aggregating within one hour. The aggregation propensity of GLP-1am is well predicted by the strength of the attractive intermolecular interactions, which are stronger for GLP-1am in pH 8 than pH 5. The nucleation-dependent kinetics at pH 8 agree with what has been observed for the non-amidated peptide sequence (21), under agitation conditions.

GLP-1am aggregation accelerates with seeding and concentration, confirming a nucleation-dependent mechanism. Under quiescent conditions and high peptide concentration, we did not observe the formation of twisted amyloid fibrils typical of cross-beta amyloid structures. A similar behaviour was shown for Aβ sequences, where an increase in concentration led to a decrease in fibrillation propensity (32, 33). At high concentrations, GLP-1am forms straight nanosheets after days of incubation at room temperature, similar to what is observed for glucagon (34). The straight morphology of these peptide assemblies must depend on GLP-1am accessing oligomeric structures, leading to a different pathway than that of amyloid formation. This contrasts with amyloid formation, which instead requires a degree of unfolding to create seeds, which are normally generated by agitation. Thus, at high peptide concentrations, GLP-1am behaves like glucagon (34) and other reversible fibrillar aggregates formed by incretin hormones (10).

The chemistry of the co-solutes reveals the nature of intermolecular interactions driving GLP-1am oligomerisation.

NaCl steadily increases GLP-1am aggregation propensity, with a corresponding decrease in the IP_{Fagg}, which can be explained by the screening of several charged patches present on the electrostatic surface of GLP-1am at pH 5 (SF9A).Direct relationships between NaCl concentration and acceleration of fibril formation have been observed before, especially for peptides (35).

Like NaCl, arginine.HCl, can negatively impact protein solubility by screening repulsive intermolecular interactions, leading to the destabilisation of proteins with high surface charge (36). We saw this effect at 50 mM arginine.HCl, where the rate of aggregation was increased. Where NaCl drove an increase in size for all GLP-1am concentrations the effect is more complex for arginine.HCl. Below 4 mg mL^{-1} GLP-1am, and when the arginine.HCl exceeded 50 mM, GLP-1am size decreased (Figure 2B). Thus, at high peptide concentrations, arginine.HCl primarily acts as a charge screen to reduce repulsion and promote self-association. At lower peptide concentrations, arginine.HCl might engage in preferential interactions with exposed aromatic, and to a lesser extent, with hydrophilic residues to reduce oligomer size (30). Depending on protein size and co-solute concentration (below or above 100 mM) (37), these interactions can stabilise or destabilise proteins. The dual effect of arginine.HCl on GLP-1am may arise from oligomers with partially buried aromatic side chains, which are more prevalent at higher peptide concentrations and permit electrostatic screening effects to dominate self-association behaviour.

Taken together, our results indicate that NaCl promotes GLP-1am oligomer growth by electrostatic screening, producing the largest increase in size and aggregation propensity. By contrast, arginine.HCl exerts a peptide and co-solute concentration-dependent effect, confirming that protein stability in the presence of co-solute is strongly influenced by polypeptide chain length and charge (38).

The trends for the diffusion interaction parameter, k_D, in the presence of co-solutes highlighted proline's ability to decrease attractive intermolecular interactions between GLP-1am molecules, and the propensity to grow into large aggregates. The mechanisms seem to involve stabilisation of early soluble oligomeric species, given that: (i) proline displays a general effect of reducing the measured R_h of GLP-1am; (ii) favours a dimeric state at low GLP-1am concentrations, and (iii) slows down the growth of aggregates. Low molecular weight species of GLP-1 analogues have been previously shown to inhibit peptide aggregation (14). Overall, the effect of proline on GLP-1am oligomerisation agrees with its ability to inhibit protein aggregation *in vivo* and *in vitro* at early stages of aggregation, but not when larger aggregates have formed (39).

The mechanism by which proline stabilises GLP-1am early oligomers might involve one or multiple properties of this co-solute. We now know that in the glucagon family, the aggregation-prone regions include aromatic and hydrophobic amino acids (the xFxxWL hexapeptide), which drive the formation of reversible amyloids, the form in which these hormones are stored in acidic secretion vesicles (40). In general, proline is excluded from the protein backbone (41) and interacts preferentially with aromatic sidechains based on the ability of the proline ring to form CH-π interactions (30, 42, 43). These properties make proline a key osmolyte for protein refolding (44, 45). Notably, proline has been shown to reduce protein-protein interactions between globular proteins (46, 47). Thus, we can

speculate that proline might favour GLP-1am conformations that are less competent to aggregate, perhaps via excluded-volume effects (48). Lastly, proline can be effective in reducing the viscosity of proteins (49), but we exclude this effect as we do not observe any peptide viscosity changes with this co-solute (SF9B-D).

The pH-dependence of proline stabilisation has been less studied; thus, it is more difficult to explain. Previous observations on monoclonal antibody stability showed that proline, at the same concentration, can inhibit aggregation at pH 5 in histidine buffer (49) where antibody aggregation was less of an issue. Thus, the activity of proline may depend on the ability of proteins to form soluble low molecular weight oligomers with specific electrophoretic properties, like those conferred by the conformation adopted by GLP-1am at low concentrations and pH 5 (Table S5). This is supported by recent evidence that osmolytes can solubilise proteins only if they possess a certain degree of globularity (50).

Overall, we have shown that the co-solute effect and their trends are reflected by the reduction in the magnitude of the negative k_D with proline, but an increase in the magnitude of the negative k_D with NaCl and arginine.HCl, when compared to GLP-1am in buffer alone. The k_D encompasses electrostatic and hydrodynamic effects, which control protein diffusion (51). In the case of proline, its low ionic strength implies that diffusion of GLP-1am is driven less by electrostatics, and more by protein-protein interactions. The presence of effective thresholds for co-solutes was previously observed also for glucagon (52) and likely reflects the dual ability of the guanidium group of arginine.HCl and proline ring (30) to engage with aromatic sidechains as well as osmolyte effects.

In conclusion, we have shown that in conditions mimicking storage in secretory granules, GLP-1am exists as soluble discrete n-mers that assemble into nanosheets in quiescent conditions, at 25 °C (Figure 5G). The addition of proline to GLP-1am solutions favours the lower oligomerisation states and delays the growth into nanostructures. Conversely, ionic co-solutes, such as NaCl or arginine.HCl, promote fast aggregation of GLP-1am indicating how screening of electrostatics promotes self-assembly. This work also shows that a combination of techniques is necessary to disentangle the complex behaviour of protein self-association mechanisms in the presence of co-solutes, and at peptide concentrations that are relevant to biology and pharmaceutical formulations. Lastly, we highlighted how the colloidal stability of a peptide can be measured by the interaction parameter, k_D. This parameter might be used to quantify how effective a co-solute will be in reducing the aggregation of a given peptide.

Experimental procedures

C-terminally amidated GLP-1am was purchased from two suppliers, GL Biochem Ltd. (Shanghai, China; batch 1) and GenScript (Hong Kong; batch 2). Both products were synthesised using solid-phase peptide synthesis, purified by reverse-phase HPLC (RP-HPLC) and supplied as acetate salts. The GL Biochem batch had a reported purity of 95.29% as evaluated by RP-HPLC. The company did not specify the residual content of counterions after purification. Two preparations were purchased from GenScript. Preparation 1 was 97.2% pure with residual content of: TFA 0.45%, acetate 0.06% and chloride 0.6%. Preparation 2 was 95.1% pure with residual content of: TFA 0.62%, acetate 1.58% and chloride 0.31%. Quality control was performed by GenScript. No further purification on either batch was performed. Preparation 1 was used for experiments in Figure 3, 4E-F, 5, S3E-F, SF6 (except for SF6C). Preparation 2 was used for experiments in SF7B-C, SF7G-I and SF8 (except for C, D).

Buffer preparation

Sodium acetate buffer (25 mM sodium acetate, pH 5) was prepared from 8 mmol sodium acetate (≥99%, Sigma-Aldrich, USA) and 4 mmol glacial acetic acid (≥99%, Thermo Fisher Scientific, USA). The solution did not require further pH adjustment. Sodium phosphate buffer (25 mM, pH 8) was prepared from 0.0016 mol of sodium phosphate monobasic anhydrous (≥99%, Sigma-Aldrich, USA) and 0.0233 mol of basic component sodium phosphate dibasic heptahydrate (ASC Grade, Sigma-Aldrich, USA). The pH was adjusted using 12.5 M sodium hydroxide.

Peptide stock preparation

GLP-1am was stored in lyophilised powder form at -20°C, in tightly sealed and parafilmed vials, in a box containing silica gel. Stock solutions were prepared freshly on the day of measurement.

GL Biochem batch (batch 1): lyophilised GLP-1am was dissolved in 25 mM acetate buffer, pH 5 where it was soluble up to 12 mg mL^{-1}. All solutions were prepared from this initial stock concentration to maintain consistency across datasets.

GenScript batch (batch 2): the lyophilised peptide from GenScript was soluble in 25 mM sodium acetate, pH 5, to a concentration of 4 mg mL^{-1} since opalescence was present from above this concentration. Warming of the stock solution to 55ºC at a rate of 1 ºC min^{-1} and holding for 1' cleared the opalescence and increased solubility up to 12 mg mL^{-1}.

Stock solutions were filtered through 0.2 µm polyethersulfone (PES) filters (Thomson, USA) before measurements. The concentration was determined by measuring the absorbance at 280 nm of the stock solutions, using a calculated theoretical extinction coefficient of 6990 M^{-1} cm^{-1}. The absorbance was measured after dilution using a NanoDrop One UV/Vis Spectrophotometer (ThermoFisher Scientific, USA) or a VersaWave UV/Vis spectrophotometer.

Co-solute stock preparation

Stocks of L-Arginine.HCl, L-Proline and NaCl (Sigma-Aldrich, USA) were made by dissolving the respective co-solute in the appropriate buffer to give a 600 mM concentration and subsequently filtered through 0.2 µm PES filters (Millex, Germany).

Dynamic light scattering (DLS) and differential scanning fluorimetry (nanoDSF)

Individual samples were prepared by dilution of peptide stock or co-solute stock in sodium acetate buffer to give the desired peptide or co-solute concentration. High-throughput combined DLS/nanoDSF measurements were performed using a Prometheus Panta (NanoTemper Technologies, Germany), which uses a 405 nm laser with a 147° scattering angle. Approximately 10 µL of sample was loaded into NanoTemper standard capillaries, and DLS was performed at 20°C with 10 acquisitions, each with an acquisition time of 5 s. Thermal stability was measured by nanoDSF, monitoring the intrinsic fluorescence at emission wavelengths of 330 and 350 nm (excitation at 280 nm) via a thermal ramp of 1°C min^{-1} from 20-95°C. The diffusion interaction parameter k_D was determined using a concentration series of 5 different peptide concentrations between 1 and 8 mg mL^{-1}, with 10 acquisitions of 5 s acquisition time. All formulations were measured in independent triplicate. The onset of aggregation was measured by monitoring turbidity and cumulant radius simultaneously. Data analysis was performed using PR.Analysis software v.1.7.1 (NanoTemper Technologies). Selected samples were measured again in low-throughput DLS using a Mobius (Wyatt Technology, USA) with a 532 nm laser at 163.5º scattering angle, more sensitive to polydisperse samples. For all samples, the dispersant viscosity (including co-solutes when appropriate) was used to calculate the hydrodynamic radii of the samples.

Diffusion Interaction parameter (k_D) determination

K_D calculations were performed using the diffusion coefficient of the major species (peak 1, R_h 2.1 nm) from the hydrodynamic radius using the Stokes-Einstein Equation:

$$D_c = \frac{k_B T}{6\pi\eta R_h}$$

Where D_c is the translational diffusion coefficient, k_B is the Boltzmann constant, T is the temperature at which the DLS was taken, η is the viscosity of the buffer, and R_h is the hydrodynamic radius. The subsequent diffusion coefficient was utilised in linear regression.

The diffusion interaction parameter was determined by linear regression of the diffusion coefficients of solutions with varying peptide concentrations, with or without co-solutes. The equation used to fit the data is:

$$D = D_0(1 + k_D c)$$

Where D is the diffusion coefficient of the peptide in solution, D_0 is the diffusion coefficient at infinite dilution and c is the concentration of the protein in solution.

A total of 5 capillaries per concentration (except for 6 mg mL^{-1}) were repeated over 2 days. Acquisitions with autocorrelation curves giving non-random residuals were excluded from the analysis. For each capillary, the average of 10 acquisitions was displayed as data point. Data fitting was performed using the linear regression function from the SciPy (v. 1.11.4)

package in Python (v. 3.11.7). The standard error was calculated by error propagation using the errors from the linear regression of the slope and the intercept.

Zeta-potential determination

Zeta potential determination was performed at 25 °C using a Mobius (Wyatt Technology, USA). All data analysis was performed using Dynamics Software Version 8.1.2.144 (Wyatt Technology, USA). The zeta potential was measured at a peptide concentration of 0.3 mg/mL in pH ranges from 3.75 to 5 (sodium acetate, 25 mM) and 6.2 to 8 (sodium phosphate, 25 mM). The electric field frequency was 10.0 Hz, and the voltage amplitude was 2.5 V.

Dispersant viscosity measurement

The viscosity of the dispersants was measured at 20 °C using the Prometheus Panta (NanoTemper Technologies) and 100 nm polystyrene 3000 Series Nanosphere™ Size Standards (Thermo Scientific, USA). Nanospheres were diluted 1:1000 into samples containing co-solute and buffer (Table S6). A buffer of known viscosity was also used as a reference, in this case it was either sodium acetate (25 mM) or Phosphate Buffered Saline. The size of the nanospheres was compared, and the following equation was used to estimate the viscosity:

$$viscosity = viscosity_{reference} \times \frac{R_h}{R_{h\,(reference)}}$$

A Honeybun rheometer (Unchained Labs, USA) was used to confirm the reliability of some of the values measured with the nanospheres. Data analysis was performed using the Honeybun software.

Kinetics of aggregation by turbidity

Kinetics of aggregation were monitored by measuring the turbidity of samples by UV Spectroscopy, either using a Cary 3500 Multicell UV-Vis Spectrophotometer (Agilent Technologies) or a FLUOstar Omega plate reader (BMG LabTech). The absorbance at 350 nm was monitored every 5 minutes, without agitation, at 25°C.

Kinetics of amyloid formation by Thioflavin T (ThT) binding and Low-Throughput Intrinsic Tryptophan Fluorescence

ThT binding was monitored using a Fluoromax 4 (Horiba). GLP-1am at 1 mg mL^{-1} was incubated with 100 μM ThT, at 37 ºC in a shaking incubator with 180 rpm. Detection of ThT binding was performed by recording the fluorescence emission at 482 nm with an excitation wavelength of 448 nm. Fluorescence was measured with a 5 nm response.

Samples containing 2 mg mL^{-1} were incubated at 25 ºC in 25 mM sodium acetate, pH 5 for 4 days. Fluorescence was recorded each day using a Fluoromax 4 (Horiba). Changes in intrinsic Trp fluorescence were recorded by measuring emission at 300-400 nm with excitation at 280 nm with a 2 nm bandwidth.

Size-exclusion chromatography (SEC) by FPLC

Analytical size-exclusion chromatography was performed using an ÄKTA Pure 25 (Cytiva, UK) using a Superdex 75 10/300 GL (Cytiva) with a flow rate of 0.7 mL/min, with the mobile phase having the same composition as the formulation buffer. Gel Filtration Calibration Kit (Low-Weight Molecular, Cytiva) containing aprotinin, ribonuclease, carbonic anhydrase and ovalbumin was run under the same elution conditions as the experiments. The molecular weight plotted as a function of elution volume ($logM = b - cV$) was used to estimate the size of the GLP-1am species present (SF4F).

Asymmetric flow field flow fractionation (AF4)

AF4-MALS was performed using an Infinity II HPLC (Agilent Technologies, USA) and a 2 kDa regenerated cellulose membrane in a variable height, short channel with a 275 µm spacer. Samples were introduced using a 1260 Vialsampler and monitored with the following in-line detectors: 1260 DAD UV/Vis spectrophotometer, 1260 Fluorescence, DAWN (Wyatt Technology) and Optilab (Wyatt Technology). Channel flow rates were controlled by an Eclipse (Wyatt Technology). The AF4 method used is in Table S7 with a focusing position of 25%.

Circular dichroism

Circular dichroism (CD) spectra were measured on a Jasco J-810 CD spectrometer (Jasco, UK). Far-UV CD spectra were measured in a 1-mm pathlength cuvette with 1-nm step size and with a 1-nm spectral bandwidth and a monomer concentration of 0.3 mg mL^{-1}. Near-UV CD spectra were measured with 1-nm step size and 1-nm spectral bandwidth in a 2-mm pathlength cuvette and a monomer concentration of 2 mg mL^{-1}. The recording was performed in step mode with 8 seconds response time. All measurements were performed at 20 °C.

The millidegree units were converted into molar ellipticity after buffer subtraction using

$$\theta = \frac{mdeg}{10 * N * c * l}$$

Where N is the number of peptide bonds, l is the pathlength in cm, and c is the concentration of peptide monomer in mol L^{-1}.

Analytical Ultracentrifugation

Sedimentation velocity analytical ultracentrifugation was performed on a Beckman Optima analytical ultracentrifuge using absorbance optics set at 290 nm. Samples were loaded into two-sector cells with quartz glass windows, and the samples were centrifuged at 50,000 RPM using an 8-hole An50Ti rotor. Scans were set to be every 60 seconds for a total of 400 scans.

Analysis was performed using Sedfit.(53) Sedimentation coefficients were corrected for buffer composition to standard conditions.

Negative Staining and Transmission Electron Microscopy

Negative staining was performed using freshly glow-discharged, carbon-coated copper grids. Sample was applied for 1.5 minutes and blotted away. Grids were washed twice with

water, followed by two washes with 0.75 % uranyl formate, with the second staining step in 0.75% uranyl formate for 20 seconds.

TEM studies were conducted using a JEOL JEM-120i electron microscope operating at 80 kV and equipped with a SightSKY (EM-04500SKY) 19 megapixel camera.

CRediT authorship contribution statement

AS – Investigation, Methodology, Formal analysis, Conceptualisation; **TAJ** – Investigation, formal analysis; **NA** Editing, Resources, Formal analysis; **RM**, **RKS**, **VL** – Project administration, Editing, Resources; **BC** and **TSW** – Writing original draft, Conceptualization, Editing, Supervision, Project administration, Funding acquisition.

Conflicts of Interests

RM, RKS, VL are employees of AstraZeneca. NBPA is an employee of NanoTemper Technologies GmbH.

Data Availability

Data are available to be shared upon request. Please contact b.ciani@sheffield.ac.uk.

Supporting Information

This article contains supporting information.

Acknowledgements

We acknowledge the BBSRC White Rose DTP and AstraZeneca for a studentship to AS (BB/T007222/1) and the Royal Society for a Short Industry Fellowship to BC (SIF\R1\241044). The Wyatt bioanalytical instrument, used in this study, is financially supported by the BBSRC ALERT scheme (BB/V019341/1), awarded to TSW and BC. We acknowledge Chris Hill and Dr Svetomir B Tzokov of the School of Biosciences Cryo-EM Facility at the University of Sheffield for support with TEM. We thank William D Mulcrone and Dr David J Reynolds for their useful discussion.

References

1. Li, B., Yang, M. Y., Kim, S.-K., and Goddard, W. A. I. (2024) The G Protein-First Mechanism for Activation of the Class B Glucagon-like Peptide 1 Receptor Coupled to N-Terminal Domain-Mediated Conformational Progression. *J. Am. Chem. Soc.* 10.1021/jacs.4c08128
2. Baggio, L. L., and Drucker, D. J. (2007) Biology of Incretins: GLP-1 and GIP. *Gastroenterology*. **132**, 2131–2157
3. Todd, J. F., and Bloom, S. R. (2007) Incretins and other peptides in the treatment of diabetes. *Diabet. Med.* **24**, 223–232
4. Yu, M., Benjamin, M. M., Srinivasan, S., Morin, E. E., Shishatskaya, E. I., Schwendeman, S. P., and Schwendeman, A. (2018) Battle of GLP-1 delivery technologies. *Adv. Drug Deliv. Rev.* **130**, 113–130
5. Zheng, Z., Zong, Y., Ma, Y., Tian, Y., Pang, Y., Zhang, C., and Gao, J. (2024) Glucagon-like peptide-1 receptor: mechanisms and advances in therapy. *Signal Transduct. Target. Ther.* **9**, 1–29
6. Wang, Y., Lomakin, A., Kanai, S., Alex, R., and Benedek, G. B. (2015) Transformation of Oligomers of Lipidated Peptide Induced by Change in pH. *Mol. Pharm.* **12**, 411–419
7. Frederiksen, T. M., Sønderby, P., Ryberg, L. A., Harris, P., Bukrinski, J. T., Scharff-Poulsen, A. M., Elf-Lind, M. N., and Peters, G. H. (2015) Oligomerization of a Glucagon-like Peptide 1 Analog: Bridging Experiment and Simulations. *Biophys. J.* **109**, 1202–1213
8. Li, Y., Shao, M., Zheng, X., Kong, W., Zhang, J., and Gong, M. (2013) Self-Assembling Peptides Improve the Stability of Glucagon-like Peptide-1 by Forming a Stable and Sustained Complex. *Mol. Pharm.* **10**, 3356–3365
9. Takeuchi, M., Okamoto, M., Okamoto, R., Kinoshita, H., Yamaguchi, Y., and Watanabe, N. (2018) Discovery of a long-acting glucagon-like peptide-1 analog with enhanced aggregation propensity. *Peptides*. **102**, 8–15
10. Maji, S. K., Perrin, M. H., Sawaya, M. R., Jessberger, S., Vadodaria, K., Rissman, R. A., Singru, P. S., Nilsson, K. P. R., Simon, R., Schubert, D., Eisenberg, D., Rivier, J., Sawchenko, P., Vale, W., and Riek, R. (2009) Functional Amyloids As Natural Storage of Peptide Hormones in Pituitary Secretory Granules. *Science*. **325**, 328–332
11. Egbu, R., Van Der Walle, C. F., Brocchini, S., and Williams, G. R. (2020) Inhibiting the fibrillation of a GLP-1-like peptide. *Int. J. Pharm.* **574**, 118923
12. Lundahl, M. L. E., Fogli, S., Colavita, P. E., and Scanlan, E. M. (2021) Aggregation of protein therapeutics enhances their immunogenicity: causes and mitigation strategies. *RSC Chem. Biol.* **2**, 1004–1020
13. Venanzi, M., Savioli, M., Cimino, R., Gatto, E., Palleschi, A., Ripani, G., Cicero, D., Placidi, E., Orvieto, F., and Bianchi, E. (2020) A spectroscopic and molecular dynamics study on the aggregation process of a long-acting lipidated therapeutic peptide: the case of semaglutide. *Soft Matter*. **16**, 10122–10131
14. Bothe, J. R., Andrews, A., Smith, K. J., Joyce, L. A., Krishnamachari, Y., and Kashi, S. (2019) Peptide Oligomerization Memory Effects and Their Impact on the Physical Stability of the GLP-1 Agonist Liraglutide. *Mol. Pharm.* **16**, 2153–2161
15. Chang, X., Keller, D., O'Donoghue, S. I., and Led, J. J. (2002) NMR studies of the aggregation of glucagon-like peptide-1: formation of a symmetric helical dimer. *FEBS Lett.* **515**, 165–170
16. Doyle, B. L., Pollo, M. J., Pekar, A. H., Roy, M. L., Thomas, B. A., and Brader, M. L. (2005) Biophysical signatures of noncovalent aggregates formed by a glucagonlike peptide-1 analog: A prototypical example of biopharmaceutical aggregation. *J. Pharm. Sci.* **94**, 2749–2763

17. Zapadka, K. L., Becher, F. J., Gomes dos Santos, A. L., and Jackson, S. E. (2017) Factors affecting the physical stability (aggregation) of peptide therapeutics. *Interface Focus*. **7**, 20170030
18. Sunde, M., Serpell, L. C., Bartlam, M., Fraser, P. E., Pepys, M. B., and Blake, C. C. F. (1997) Common core structure of amyloid fibrils by synchrotron X-ray diffraction1. *J. Mol. Biol.* **273**, 729–739
19. Parker, J. c., Andrews, K. m., Rescek, D. m., Massefski Jr, W., Andrews, G. c., Contillo, L. g., Stevenson, R. w., Singleton, D. h., and Suleske, R. t. (1998) Structure-function analysis of a series of glucagon-like peptide-1 analogs. *J. Pept. Res.* **52**, 398–409
20. Miranda, L. P., Winters, K. A., Gegg, C. V., Patel, A., Aral, J., Long, J., Zhang, J., Diamond, S., Guido, M., Stanislaus, S., Ma, M., Li, H., Rose, M. J., Poppe, L., and Véniant, M. M. (2008) Design and Synthesis of Conformationally Constrained Glucagon-Like Peptide-1 Derivatives with Increased Plasma Stability and Prolonged in Vivo Activity. *J. Med. Chem.* **51**, 2758–2765
21. Zapadka, K. L., Becher, F. J., Uddin, S., Varley, P. G., Bishop, S., Gomes dos Santos, A. L., and Jackson, S. E. (2016) A pH-Induced Switch in Human Glucagon-like Peptide-1 Aggregation Kinetics. *J. Am. Chem. Soc.* **138**, 16259–16265
22. Přáda Brichtová, E., Krupová, M., Bouř, P., Lindo, V., Gomes dos Santos, A., and Jackson, S. E. (2023) Glucagon-like peptide 1 aggregates into low-molecular-weight oligomers off-pathway to fibrillation. *Biophys. J.* 10.1016/j.bpj.2023.04.027
23. Dauer, K., Kamm, W., Wagner, K. G., and Pfeiffer-Marek, S. (2021) High-Throughput Screening for Colloidal Stability of Peptide Formulations Using Dynamic and Static Light Scattering. *Mol. Pharm.* **18**, 1939–1955
24. Garidel, P., Blume, A., and Wagner, M. (2015) Prediction of colloidal stability of high concentration protein formulations. *Pharm. Dev. Technol.* **20**, 367–374
25. Maji, S. K., Schubert, D., Rivier, C., Lee, S., Rivier, J. E., and Riek, R. (2008) Amyloid as a Depot for the Formulation of Long-Acting Drugs. *PLOS Biol.* **6**, e17
26. Fleming, P. J., and Fleming, K. G. (2018) HullRad: Fast Calculations of Folded and Disordered Protein and Nucleic Acid Hydrodynamic Properties. *Biophys. J.* **114**, 856–869
27. Yadav, S., Liu, J., Shire, S. J., and Kalonia, D. S. (2010) Specific interactions in high concentration antibody solutions resulting in high viscosity. *J. Pharm. Sci.* **99**, 1152–1168
28. He, F., Woods, C. E., Becker, G. W., Narhi, L. O., and Razinkov, V. I. (2011) High-Throughput Assessment of Thermal and Colloidal Stability Parameters for Monoclonal Antibody Formulations. *J. Pharm. Sci.* **100**, 5126–5141
29. Vivian, J. T., and Callis, P. R. (2001) Mechanisms of Tryptophan Fluorescence Shifts in Proteins. *Biophys. J.* **80**, 2093–2109
30. Cloutier, T. K., Sudrik, C., Mody, N., Hasige, S. A., and Trout, B. L. Molecular computations of preferential interactions of proline, arginine.HCl, and NaCl with IgG1 antibodies and their impact on aggregation and viscosity. *mAbs*. **12**, 1816312
31. Ng, Y. K., and Konermann, L. (2024) Mechanism of Protein Aggregation Inhibition by Arginine: Blockage of Anionic Side Chains Favors Unproductive Encounter Complexes. *J. Am. Chem. Soc.* **146**, 8394–8406
32. Nick, M., Wu, Y., Schmidt, N. W., Prusiner, S. B., Stöhr, J., and DeGrado, W. F. (2018) A long-lived Aβ oligomer resistant to fibrillization. *Biopolymers*. **109**, e23096
33. Hasecke, F., Miti, T., Perez, C., Barton, J., Schölzel, D., Gremer, L., Grüning, C. S. R., Matthews, G., Meisl, G., Knowles, T. P. J., Willbold, D., Neudecker, P., Heise, H., Ullah, G., Hoyer, W., and Muschol, M. (2018) Origin of metastable oligomers and their effects on amyloid fibril self-assembly. *Chem. Sci.* **9**, 5937–5948
34. Andersen, C. B., Otzen, D., Christiansen, G., and Rischel, C. (2007) Glucagon Amyloid-like Fibril Morphology Is Selected via Morphology-Dependent Growth Inhibition. *Biochemistry*. **46**, 7314–7324

35. Buell, A. K., Hung, P., Salvatella, X., Welland, M. E., Dobson, C. M., and Knowles, T. P. J. (2013) Electrostatic Effects in Filamentous Protein Aggregation. *Biophys. J.* **104**, 1116–1126
36. Prašnikar, M., Proj, M., Bjelošević Žiberna, M., Lebar, B., Knez, B., Kržišnik, N., Roškar, R., Gobec, S., Grabnar, I., Žula, A., and Ahlin Grabnar, P. (2024) The search for novel proline analogs for viscosity reduction and stabilization of highly concentrated monoclonal antibody solutions. *Int. J. Pharm.* **655**, 124055
37. Platts, L., and Falconer, R. J. (2015) Controlling protein stability: Mechanisms revealed using formulations of arginine, glycine and guanidinium HCl with three globular proteins. *Int. J. Pharm.* **486**, 131–135
38. Kaushik, J. K., and Bhat, R. (2003) Why Is Trehalose an Exceptional Protein Stabilizer?: AN ANALYSIS OF THE THERMAL STABILITY OF PROTEINS IN THE PRESENCE OF THE COMPATIBLE OSMOLYTE TREHALOSE *. *J. Biol. Chem.* **278**, 26458–26465
39. Ignatova, Z., and Gierasch, L. M. (2006) Inhibition of protein aggregation in vitro and in vivo by a natural osmoprotectant. *Proc. Natl. Acad. Sci.* **103**, 13357–13361
40. Horváth, D., Dürvanger, Z., K. Menyhárd, D., Sulyok-Eiler, M., Bencs, F., Gyulai, G., Horváth, P., Taricska, N., and Perczel, A. (2023) Polymorphic amyloid nanostructures of hormone peptides involved in glucose homeostasis display reversible amyloid formation. *Nat. Commun.* **14**, 4621
41. Arakawa, T., and Timasheff, S. N. (1985) The stabilization of proteins by osmolytes. *Biophys. J.* **47**, 411–414
42. Biedermannova, L., Riley, K. E., Berka, K., Hobza, P., and Vondrasek, J. (2008) Another role of proline: stabilization interactions in proteins and protein complexes concerning proline and tryptophane. *Phys. Chem. Chem. Phys.* **10**, 6350–6359
43. Zondlo, N. J. (2013) Aromatic–Proline Interactions: Electronically Tunable CH/π Interactions. *Acc. Chem. Res.* **46**, 1039–1049
44. Bartlett, G. J., Choudhary, A., Raines, R. T., and Woolfson, D. N. (2010) n→π* interactions in proteins. *Nat. Chem. Biol.* **6**, 615–620
45. Shoulders, M. D., Hodges, J. A., and Raines, R. T. (2006) Reciprocity of Steric and Stereoelectronic Effects in the Collagen Triple Helix. *J. Am. Chem. Soc.* **128**, 8112–8113
46. Mao, T., Xu, X., Winkler, P. M., Siri, C., Poliukhina, E., Silva, P. J., Xu, N., Hu, Y., Al Zahabi, K., La Polla, R., Luo, Z., Ong, Q., Alexander-Katz, A., and Stellacci, F. (2025) Stabilizing effect of amino acids on protein and colloidal dispersions. *Nature*. 10.1038/s41586-025-09506-w
47. Winkler, P. M., Siri, C., Buczkowski, J., Silva, J. V. C., Bovetto, L., Schmitt, C., and Stellacci, F. (2024) Modulating Weak Protein–Protein Cross-Interactions by the Addition of Free Amino Acids at Millimolar Concentrations. *J. Phys. Chem. B*. **128**, 7199–7207
48. Manning, M. C., Holcomb, R. E., Payne, R. W., Stillahn, J. M., Connolly, B. D., Katayama, D. S., Liu, H., Matsuura, J. E., Murphy, B. M., Henry, C. S., and Crommelin, D. J. A. (2024) Stability of Protein Pharmaceuticals: Recent Advances. *Pharm. Res.* **41**, 1301–1367
49. Hung, J. J., Dear, B. J., Dinin, A. K., Borwankar, A. U., Mehta, S. K., Truskett, T. T., and Johnston, K. P. (2018) Improving Viscosity and Stability of a Highly Concentrated Monoclonal Antibody Solution with Concentrated Proline. *Pharm. Res.* **35**, 133
50. Pepelnjak, M., Velten, B., Näpflin, N., von Rosen, T., Palmiero, U. C., Ko, J. H., Maynard, H. D., Arosio, P., Weber-Ban, E., de Souza, N., Huber, W., and Picotti, P. (2024) In situ analysis of osmolyte mechanisms of proteome thermal stabilization. *Nat. Chem. Biol.* **20**, 1053–1065
51. Sorret, L. L., DeWinter, M. A., Schwartz, D. K., and Randolph, T. W. (2016) Challenges in Predicting Protein-Protein Interactions from Measurements of Molecular Diffusivity. *Biophys. J.* **111**, 1831–1842
52. Pedersen, J. S., Dikov, D., Flink, J. L., Hjuler, H. A., Christiansen, G., and Otzen, D. E. (2006) The Changing Face of Glucagon Fibrillation: Structural Polymorphism and Conformational Imprinting. *J. Mol. Biol.* **355**, 501–523

53. Schuck, P. (2000) Size-Distribution Analysis of Macromolecules by Sedimentation Velocity Ultracentrifugation and Lamm Equation Modeling. *Biophys. J.* **78**, 1606–1619

Figure 1. Self-association of GLP-1am in 25 mM sodium acetate, pH 5. (A) Apparent hydrodynamic radius, R_h, of peak 1 (see SF1E for peak labels), and (B) corresponding polydispersity index, PDI, of GLP-1am in 25 mM acetate buffer pH 5 and 20 °C as function of its concentration measured with the Prometheus Panta (NanoTemper). The PDI is always lower than the 0.2 limit for a monodisperse sample. (C) Diffusion coefficient of the main GLP-1am species (peak 1) as a function of GLP-1am concentration. A total of 5 capillaries per concentration (except for 6 mg mL^{-1}) were repeated over 2 days. For each capillary, the average of 10 acquisitions was displayed as data point. (D) Inflection points of the 350 nm to 330 nm intrinsic fluorescence emission ratio (IP_{Fagg}) of GLP-1am as function of peptide concentration. No inflection point could be seen below 4 mg mL^{-1}, see SF3A for raw traces. (E) Two inflection points (IP) mark the appearance of turbidity during thermal ramp (1 °C min^{-1},) in GLP-1am samples from 4 mg mL^{-1}. The IP at lower temperature (T_{agg2}, squares) decreases with increasing peptide concentration, whilst the IP at higher temperature (T_{agg1}, circles) increases. See the corresponding raw data in SF3C. (F) The inflection point temperature (IP_{Fagg}) for the ratio between the intrinsic fluorescence at 350 nm and 330 nm (dashed line) corresponds to the first increase in turbidity for GLP-1am 8 mg mL^{-1}. Average and standard deviation of 3 repeats shown.

Figure 2. Apparent hydrodynamic radius of GLP-1am as function of peptide concentration in the presence of (A) sodium chloride, (B) arginine.HCl and (C) proline. A Welch's t-test, comparing pooled proline and acetate data for concentrations ≥2 mg mL^{-1}, found a significant effect of the co-solute (Welch's $t(14.4) = 2.59$, $p=0.011$, Cohen's $d = 0.822$). Inflection points for the 350 nm to 330 nm ratio of the intrinsic fluorescence emission of GLP-1am as function of peptide concentration in (D) sodium chloride, (E) arginine.HCl and (F) proline. Onset temperature for the turbidity of GLP-1am as function of peptide concentration in (G) sodium chloride, (H) arginine.HCl and (I) proline. All samples in 25 mM acetate buffer pH 5. Average and standard deviation of 3 repeats shown. Peptide concentration: 8 mg mL^{-1} (circle, yellow), 6 mg mL^{-1} (square, orange), 4 mg mL^{-1} (diamond, pink) 2 mg mL^{-1} (triangle, purple), 1 mg mL^{-1} (cross, blue). Samples prepared in acetate buffer alone are shown in black.

Figure 3. (A) AF4-MALS analysis of a 1-4 mg mL^{-1} GLP-1am fresh samples in 25 mM acetate buffer pH 5. The molecular weight determination can be found in Table S2. (B) Sedimentation velocity analytical ultracentrifugation (SV-AUC) of GLP-1am 2 mg mL^{-1} without and with 100 mM proline, in 25 mM acetate buffer at pH 5. (C) SV-AUC of GLP-1am 4 mg mL^{-1} in 25 mM acetate buffer at pH 5, without and with 100 mM proline. SV-AUC analysis in Table S3. (D-E) Aggregation kinetics of 2 mg mL^{-1} GLP-1am in 25 mM acetate buffer pH 5 without and with co-solutes monitored by apparent absorbance at 350 nm, at 25°C, in quiescent conditions. Average and standard deviation of 2 technical repeats shown in D. (F) Aggregation kinetics of 1 mg mL^{-1} GLP-1am monitored by Thioflavin T binding, at 25°C, with agitation.

Figure 4. Difference in IP temperature for the appearance of the major turbidity transition (T_{agg1}) for GLP-1am samples with excipient to those in 25 mM acetate buffer only at pH 5 at (A) 4 mg mL^{-1}, (B) 6 mg mL^{-1}, (C) 8 mg mL^{-1}. A positive difference indicates a higher temperature for aggregate formation in the presence of excipient, hence, a lower propensity to aggregate. (D) Diffusion interaction parameter, k_D, for GLP-1am in formulation with 25 mM acetate buffer pH 5 and excipients. The data displayed are from the linear regression of individual diffusion coefficients in varying co-solute concentrations, performed as indicated in materials and methods. Average and standard deviation of 3 repeats shown. (E) SEC of GLP-1am prepared without or with 100 mM proline. The samples were separated with a Superdex 75 10/300 GL at 0.7 mL min^{-1} in 25 mM acetate buffer pH 5 mobile phase, without or with 100 mM proline as appropriate (0.5 mL of 0.3 mg mL^{-1} injection). Molecular weight estimations can be found in Table S4. (F) Near UV circular dichroism of 2 mg mL^{-1} GLP-1am in 25 mM acetate buffer in the absence, or presence of 100 mM proline.

Figure 5. Transmission electron microscopy and width binned distribution of the nanosheets formed from 2 mg mL^{-1} GLP-1am incubated at 25 °C, without agitation, for 18 hours in: (A, D) 25 mM acetate buffer pH 5 (n=19); (B, D) 25 mM acetate buffer pH 5 with 50 mM arginine.HCl (n=21; (C, E) 25 mM acetate buffer pH 5 with 100 mM proline (n=27). Scale bar 500 nm. Three measurements per

nanosheet were taken (2 at the edges and one in the middle of each structure measured). (G) Oligomerisation pathway under quiescent and agitated conditions for GLP-1am at pH5. Under quiescent conditions (–agitation, top pathway), GLP-1am exists as 2-mers and 3-mers (as detected by SEC and AF4-MALS). These species grow into 4-mers and then 8/9-mer and 13/14-mer species (characterised by SV-AUC), which ultimately associate into nanosheets. Ionic co-solutes (NaCl, arginine.HCl) accelerate nanosheet formation, implying electrostatics screening as a driver of aggregation. Conversely, the presence of proline delays growth into aggregates. Under agitated conditions (+ agitation, bottom pathway), GLP-1am forms protofibrils, which subsequently mature into amyloid structures (this work and ref 21). The arrows indicate inferred transitions between experimentally observed states.

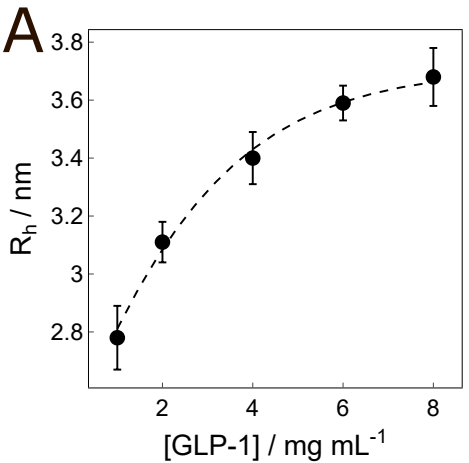

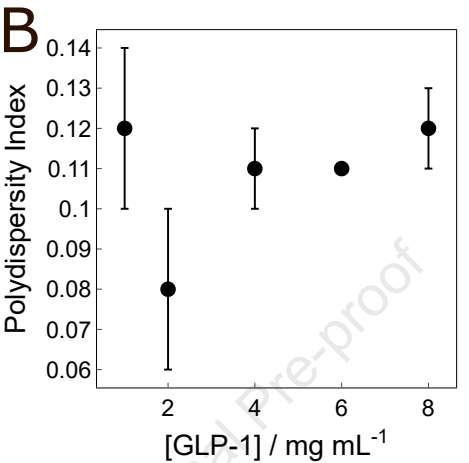

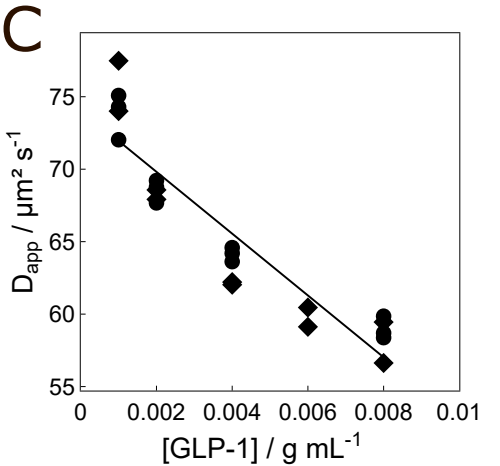

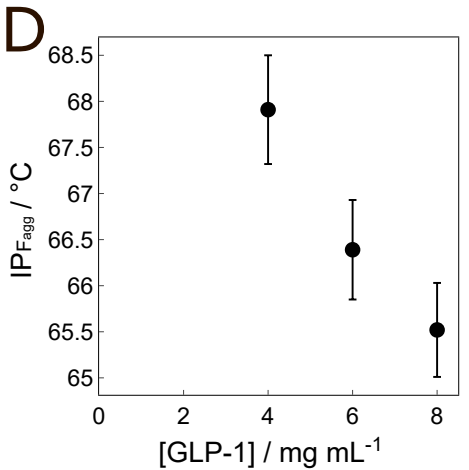

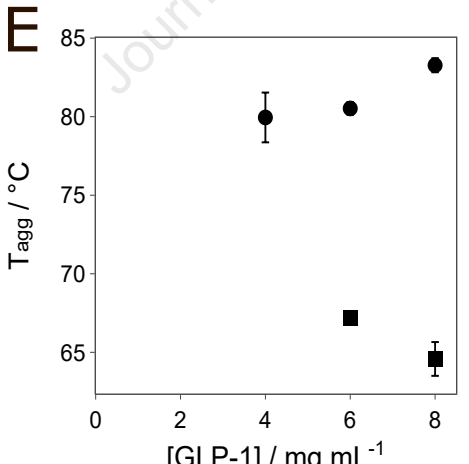

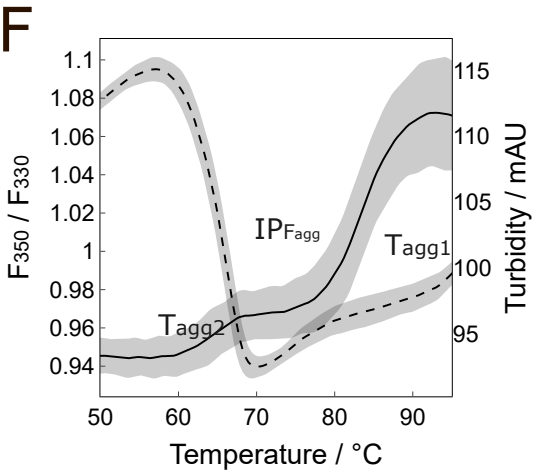

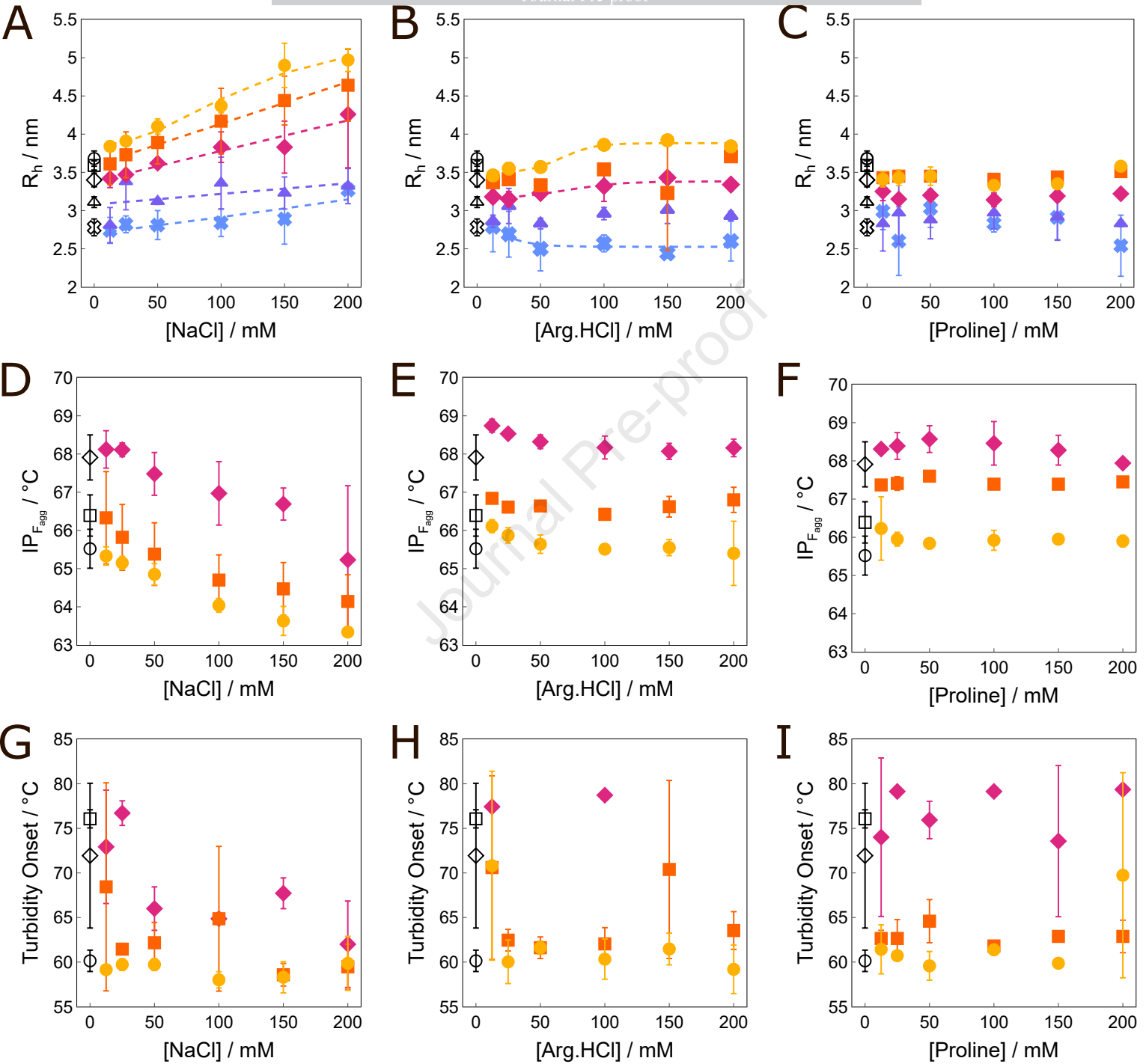

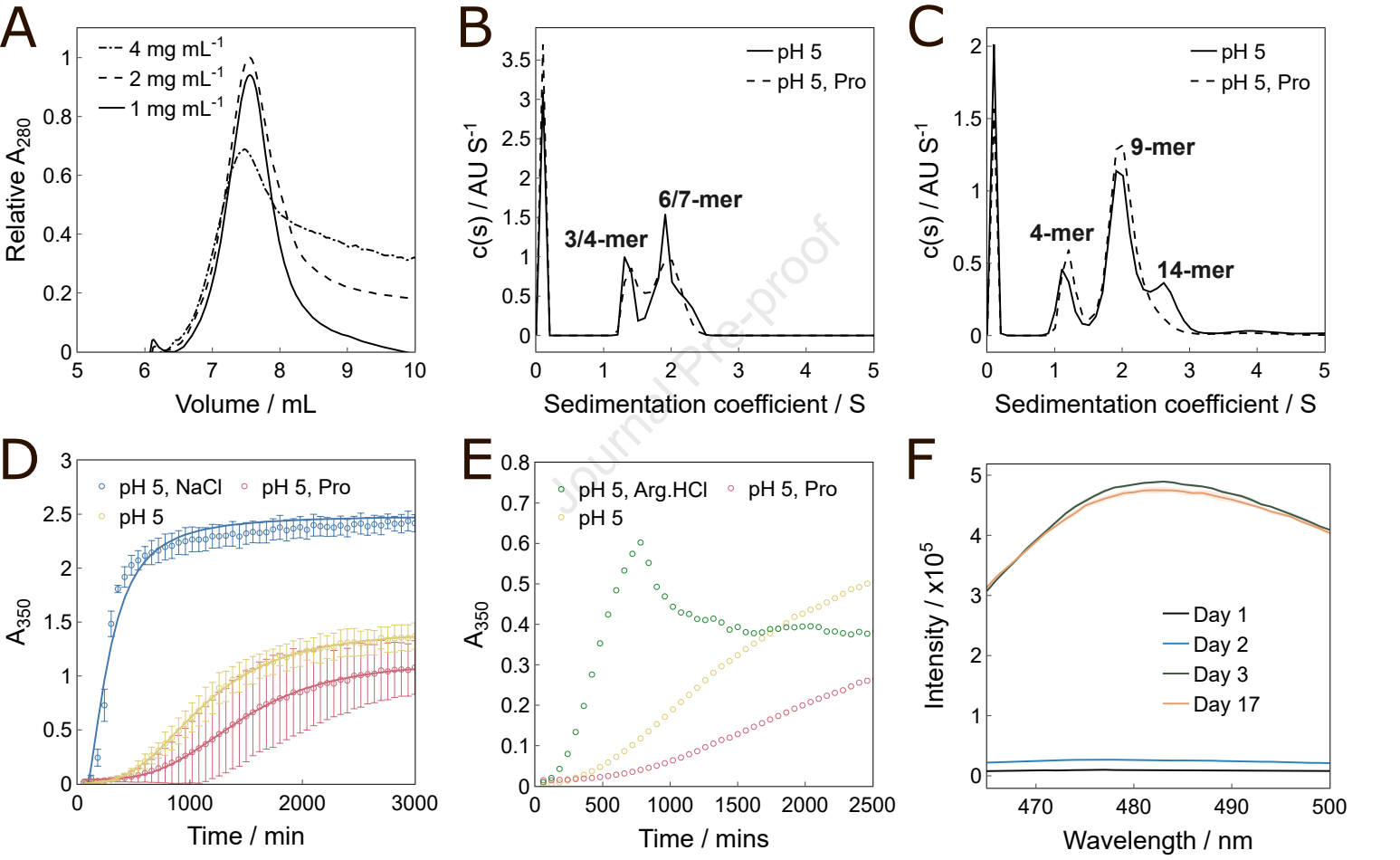

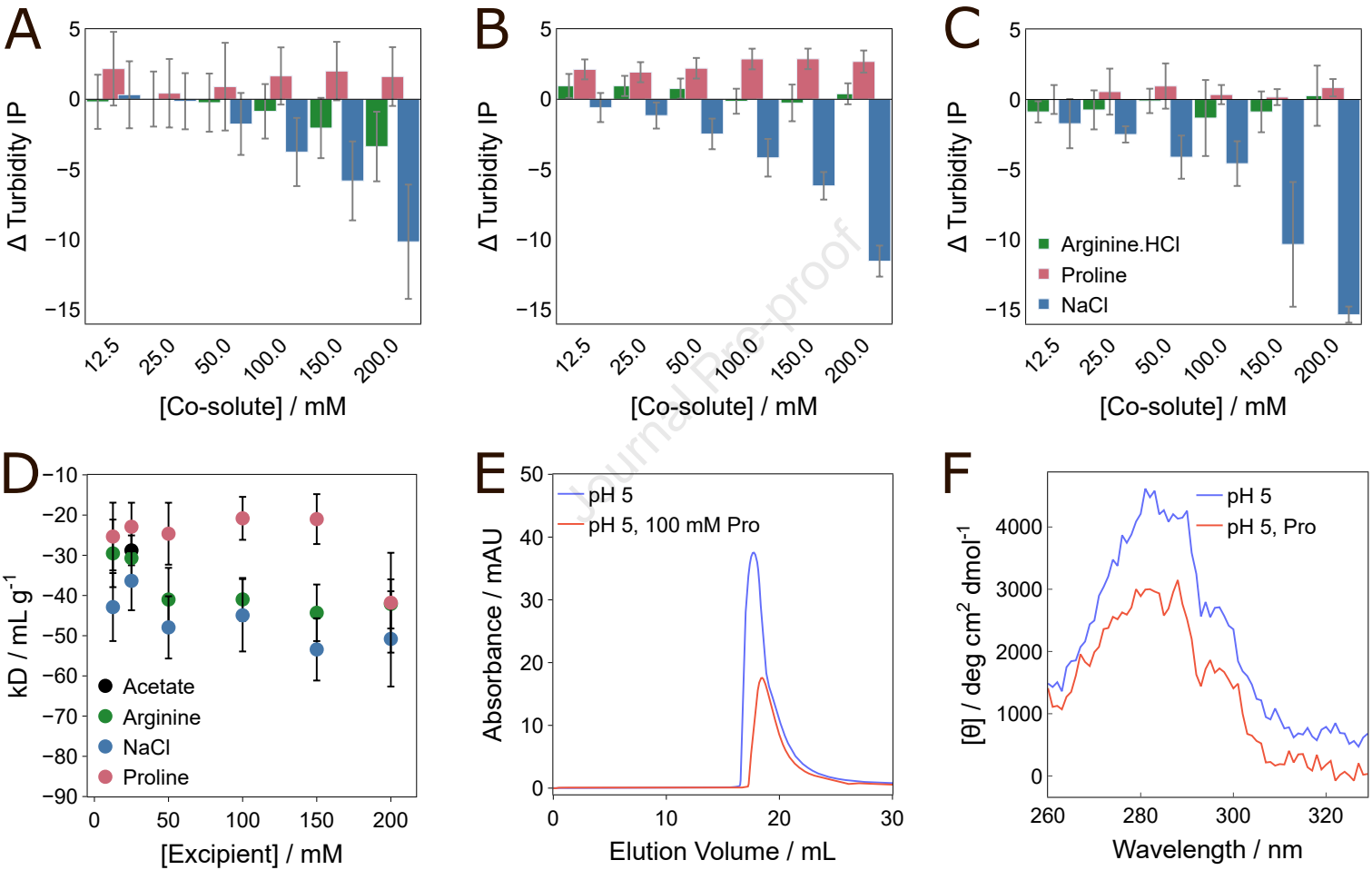

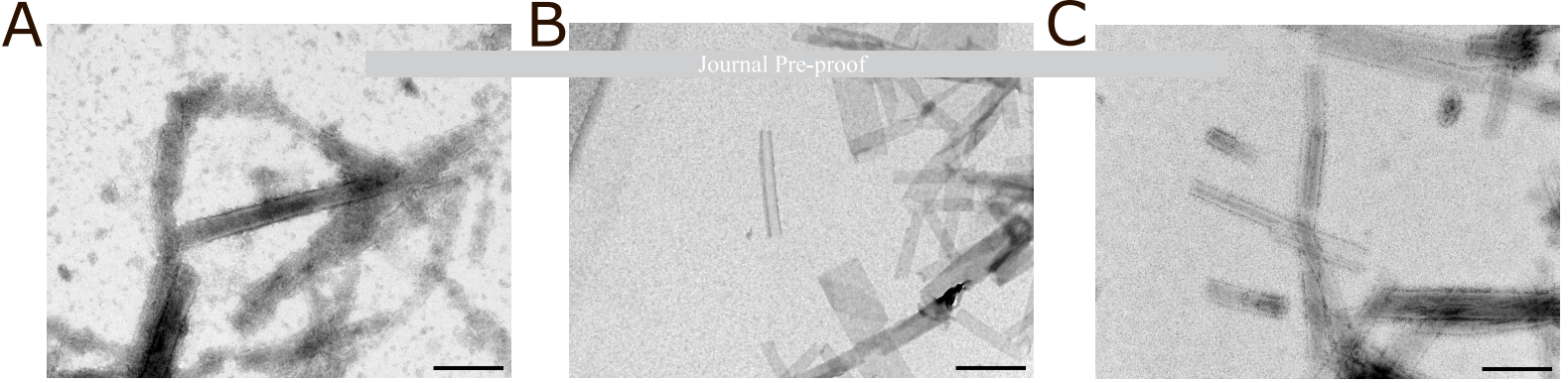

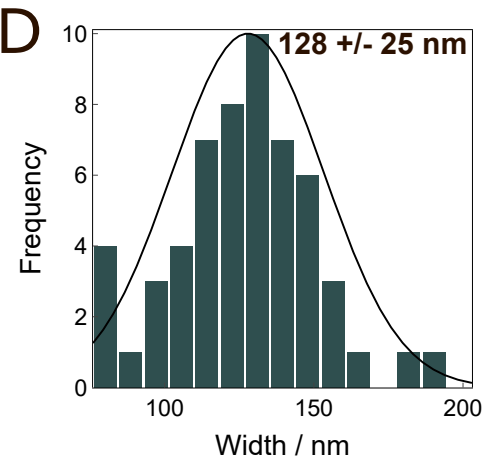

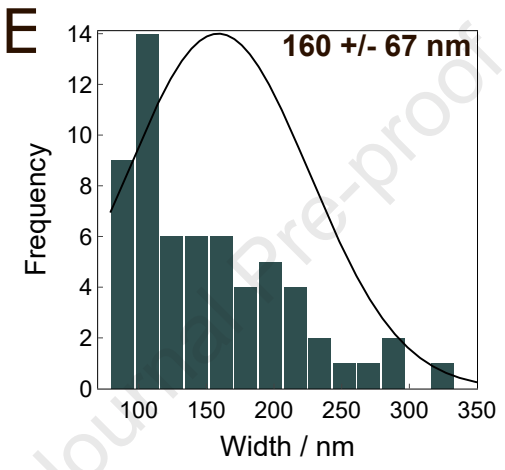

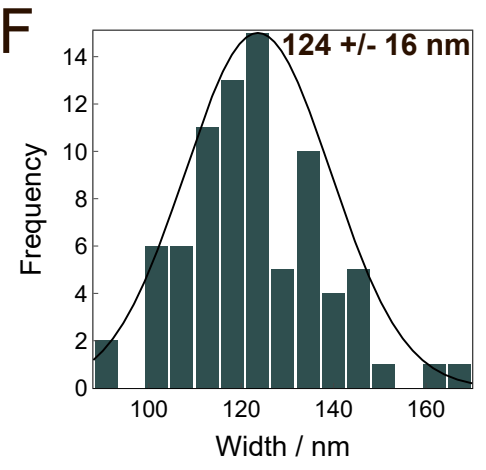

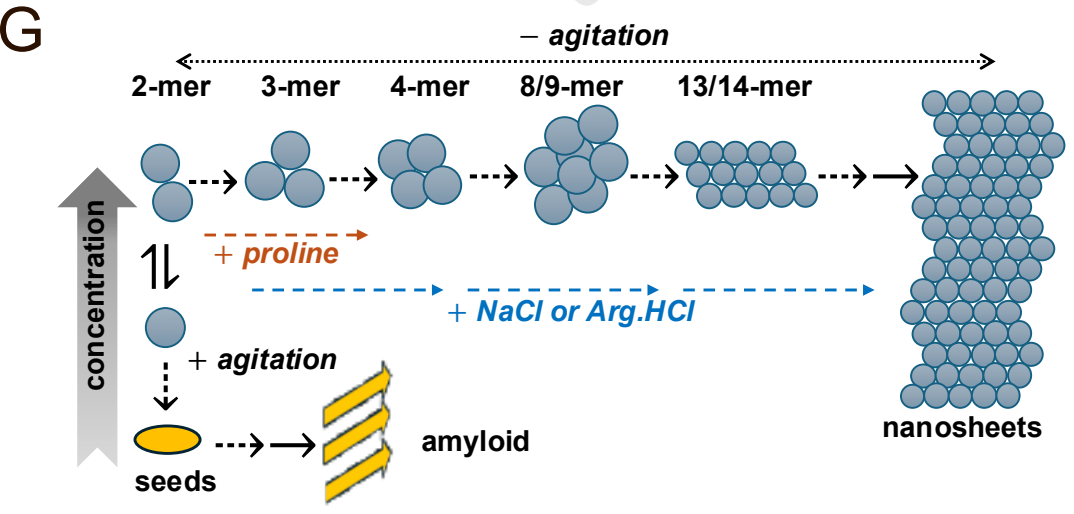

Declaration of Interest Statement

☐ The authors declare that they have no known competing financial interests or personal relationships that could have appeared to influence the work reported in this paper.

☐ The author is an Editorial Board Member/Editor-in-Chief/Associate Editor/Guest Editor for this journal and was not involved in the editorial review or the decision to publish this article.

☒ The authors declare the following financial interests/personal relationships which may be considered as potential competing interests:

Rahul Mishra, Ramesh Kumar Shanmugam, Viv Lindo are employees of AstraZeneca. Nathan Adams is an employee of NanoTemper Technologies GmbH.